Privacy-Preserving Absence Confirmation in Sensitive Nuclear Facilities

Eric Lepowsky[1,2,†]   David Snyder[1,3,†]   Alexander Glaser[1,2]   Anirudha Majumdar[1,3]

Abstract— Radioactive source term estimation is applicable to domains ranging from disaster response to nuclear monitoring. Robotic inspectors have been proposed, and in some cases deployed, for this task in certain applications; however, they have not been actively considered in nuclear verification contexts where privacy concerns are of the utmost importance. There are strict constraints on sensors and stored information due to the potentially secret nature of observable features in inspected sites. Confirming the absence of radioactive sources avoids direct observation of sensitive items, but this task has not yet been implemented with a robotic inspector. We propose a minimally-intrusive robotic verification procedure that confirms the absence of radioactive sources without requiring, nor providing, any information about the search environment. We provide theoretical guarantees on the privacy and correctness of our random walk-based approach, which are validated by extensive simulated and experimental demonstrations.

I. INTRODUCTION

Nuclear safeguards and arms control are cornerstones of the broader global security mission. Safeguards, which are measures to verify that nuclear facilities are not misused and nuclear material is not diverted from peaceful uses, require verification throughout the nuclear fuel cycle [1], [2]. Arms control, which is concerned with limiting arms competition and regulating arsenals, is made possible through declarations, data exchange, and inspections to verify compliance with agreed upon limits [3]–[5].

Onsite inspections play an important role in safeguards and arms control verification. Inspection tasks may include a variety of typically human-based measures, including verification of tags and seals, counting of objects, and, of principle interest here, radiation measurements. In scenarios where no radioactive sources (e.g., nuclear weapons or enriched uranium) are declared, the ability to identify anomalies could be crucial for verifying compliance with safeguards and arms control agreements. Furthermore, future agreements will likely require new verification approaches that minimize the need for human access to sites, such as storage or dismantlement facilities, and treaty accountable items [6].

The introduction of robotics to the field of nuclear verification has the potential to fundamentally improve and transform the efficiency, effectiveness, and capability of relevant inspection approaches [7]–[10]. A "robotic inspector" enables remote inspections so that human inspectors need not be physically present onsite, thereby reducing safety and security concerns while improving costs and timeliness.

Corresponding Author: lepowsky@princeton.edu. [1]Mechanical and Aerospace Engineering, Princeton University, NJ, USA. [2]Program on Science and Global Security (SGS), Princeton, NJ, USA. [3]Intelligent Robot Motion (IRoM) Lab, Princeton, NJ, USA. [†]E. L. and D. S. contributed equally; other authors listed alphabetically.
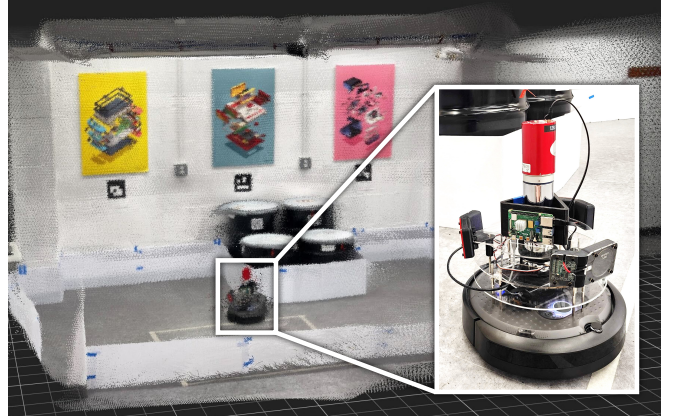
Fig. 1: **Robotic inspector in a representative laboratory search environment.** The test environment shown is approximately 15 m^2 with steel drum obstacles; dividers are used to reconfigure the space for varied test environments which are unknown to the inspector. The robotic inspector is comprised of a Create 3 platform fitted with a sodium iodide scintillator detector and Geiger counters. The inspector performs a heterogeneous random walk to explore the space while confirming the absence or presence of a radioactive source using only non-sensitive information.

Although robotic systems have been proposed, and in some cases deployed, for applications in nuclear disaster response and facility monitoring [11]–[13], there remain significant hurdles for deployment in safeguards and treaty verification. Perhaps most prominently, no sensitive information from the host site shall be unnecessarily or inadvertently revealed to the inspector. We assume that the environment layout and other observable features in the inspected site – which may include photos, dimensions, radiation measurements, etc. – are considered sensitive. Many robot-compatible methods are in contention with this requirement by either using *a priori* knowledge of the environment or, by consequence of the algorithmic design, revealing the site's configuration or radiation field *a posteriori* [14]–[21].

We also note that current approaches do not consider the inverse problem of confirming the *absence* of sources. Rather than localizing or identifying the presence of sources, which inherently requires acquiring and storing radiation measurements, confirming the absence of sources can be non-intrusive by design and avoids radiation measurements on potentially sensitive items [22]. In bringing absence confirmation to the robotics domain, we also take inspiration from the concept of "forgetting," often cited in human-robot interaction contexts [23], by implementing a more extreme alternative: never learning or remembering in the first place. With this motivation, we seek a high-confidence approach to confirm the absence of radioactive sources that neither reveals nor stores any sensitive information.

Statement of contributions. The primary contribution of this work is the development of a minimally-intrusive algorithm for confirming the absence of sources. Although the use case motivating this work and demonstrated here is specific to nuclear verification, the proposed approach can be adapted to secure inspections of other scalar fields, such as sound sources, gas leaks, aerosols, or any other emissions of interest where the signal drops with distance from the source. Guarantees on privacy preservation and bounds on the false positive rate are proven theoretically. Further, the false negative rate is characterized in terms of several parameters fundamental to the inspection task. Validation of the algorithm is undertaken in simulation and through extensive hardware experiments.

II. RELATED WORK

Radioactive source term estimation. Several methods, both for discrete source localization and distributed field mapping, have been reported which would be compatible with robotic radiation detection, including Bayesian methods [24]–[27], maximum likelihood estimation [28], [29], and machine learning [30], [31]. Mapping inherently generates a potentially sensitive result, since the inspecting party may not be privy to the configuration or layout of the search environment. A map representation of the environment can also be deduced from certain source localization methods. In the event that a source is present, the location and identifiable characteristics may be revealed. While leveraging scene understanding may improve accuracy or speed [32], [33], commensurate attention has not been given to the opposite problem of completing the task with minimal information, which would be critical for verification applications.

Minimal-information decision making. Techniques like dimensionality reduction (e.g., via encoders) [34]–[37] and control-theoretic methods [38], [39] promote robustness via lossy, compressed representations of the sensory feedback and regularization of information usage. Additionally, explicit analytical frameworks of "available information" [40], [41] quantify and formalize a relation between available and utilized information and performance. Our task falls on the extreme of this spectrum; concretely: can the source detection task be solved (in a predictable, theoretically-validated manner) with minimal (zero) information leakage? In this vein, the literature on differential privacy [42]–[44] is closely related in providing sufficient notions of information "security." However, it cannot account for the *performance* requirements demanded by our application.

Random walks. The algorithm that we propose guarantees exploration via random walk processes, for which the literature is exceedingly rich. Worst-case results for the expected cover time of walks on undirected graphs have been given in [45], [46]. General properties for finite graphs with a multitude of structures have been shown in [47]–[51], with classical Perron-Frobenius theory summarized in [52], [53]. More recent interest has been toward developing approximations to expected cover times, as in [54]–[56].

III. PROBLEM FORMULATION

Assume that a site is declared (by the host) to contain no radioactive sources. The inspection task is to verify the declaration, which requires confirming the absence of sources (or to confirm their presence in a non-compliance situation) by traversing the free space and measuring the observed radiation field. Complicating this is a crucial security constraint: the capacity of the robotic inspector to gather and retain information (any observable characteristics or features of the environment) must be kept to a minimum. Ideal verification methods must allow for both *calibrated correctness* (being able to choose the probability that the robot will return the correct inspection result) and *provable privacy* (minimizing the robot's capacity to "leak" information).

A. Environment Definition

Define an environment $E(\mathcal{I}, s, M)$, in which a robotic inspector $\mathcal{I}$ is tasked with determining the presence or absence of a radioactive source of strength $s \geq 0$ in the environment map M. Key physical parameters are defined as follows: the robotic inspector $\mathcal{I}$ has a fundamental length $r_I > 0$ (e.g., its diameter); source strength is non-negative, with $s = 0$ corresponding to the case of "no source"; map $M(l_x, l_y, B)$ is physically bounded by (known, non-sensitive) positive length constants l_x, l_y, has Poisson-distributed (i.i.d.) background radiation of mean $B \geq 0$, and has an (unknown) occupancy function defining the free space.

B. Map Compression

For this work, we must restrict ourselves to the class of maps with a single, traversable (i.e., contiguous) region of free space. Additionally, we regularize the set of valid maps by discretizing the problem into a directed graph representation, where each bin (node) is a region of space. Specifically, we will need the inequalities of Eq. 1 to hold for the discretization length ϵ_M of map M, where r_D is the detector range, or the distance from which a source is readily detectable above background. We take r_D to be the distance at which the signal-to-background ratio reaches unity.

$$r_I \leq \epsilon_M \leq \frac{r_D}{\sqrt{2}} \tag{1}$$

The left-hand inequality ensures that traversability is preserved in the discretization process, while the right-hand inequality ensures that if the robot enters a particular bin, it can detect a source from anywhere else in that bin. Consequently, each time the discretized space is covered, there must be at least one potential anomalous measurement if a source is present. We note that r_I and r_D are non-sensitive and known prior to the inspection (App. VIII-A).

Henceforth, we will refer to a *compressed map* as $M(l_x, l_y, B, \epsilon_M)$ and define a class of compressed maps as $\mathbb{M}(l_x, l_y, B, \epsilon_{\underline{M}}) = \{M(l_x, l_y, B, \epsilon_M) : \epsilon_M \geq \epsilon_{\underline{M}}\}$. The property $\epsilon' \geq \epsilon \implies \mathbb{M}(l_x, l_y, B, \epsilon') \subseteq \mathbb{M}(l_x, l_y, B, \epsilon)$ follows directly, yielding a clean subset relation. Incorporating Eq. 1, the valid set of maps for a given inspector is the set difference $\mathbb{M}_{\mathcal{I}} = \{\mathbb{M}(l_x, l_y, B, r_I) \setminus \mathbb{M}(l_x, l_y, B, \frac{r_D}{\sqrt{2}})\}$.

Importantly, although the inspector acts in $M \in \mathbb{M}_{\mathcal{I}}$, it does not see nor construct a representation of the underlying map; furthermore, to maintain the privacy of the host site, the inspector does not collect or store information (e.g., a state history) which would be sufficient to deduce the map. We emphasize that all map-dependent results presented in this paper (including coverage times) are from an omniscient view *unavailable to the inspector*.

C. Source Detection with Limited Information

The verification task considered in this work (confirming the absence of sources) has two distinct failure modes. To minimize the false negative rate (FNR) – i.e., returning "no source" when a source is present – the robot needs to guarantee exploration of the space. To control the false positive rate (FPR) – returning "source" when no source is present – each behavior indicative of source-presence must individually have a guaranteed FPR. This is similar to a standard suite of problems in robotics, including out-of-distribution (OOD) detection, anomaly detection, and failure prediction [57]–[61], among others. What distinguishes our setting, however, is the additional fundamental constraint that the stored information $\mathcal{G}_t$ be exclusively non-sensitive, that it not allow for reconstruction of the underlying map, and that this property hold uniformly across all $t \in \mathbb{N}$.

To formalize the constraint, we specify the information *available* to the robotic inspector. First, given the known r_I and r_D, it is assumed that the map M is indeed drawn from the class of valid maps $\mathbb{M}_{\mathcal{I}}$.[1] Second, the measurement model is Poisson-distributed: $h \sim \mathcal{P}(B + g(s, x, y))$. The non-negative function g is 0 if $s = 0$ or the robot position (x, y) does not have line-of-sight to the source; otherwise, $g \propto \frac{s}{r^2}$, where r is the Euclidean distance from the inspector to the source. Critically, the actual measurements h_t acquired are considered sensitive and cannot be directly stored; any trace of their history must be filtered in a sufficiently lossy fashion. Further, the robot's position cannot be known during operation, as this would reveal information about the map.

Therefore, the verification algorithm $\mathcal{A}$ must take physical actions a_t and make decisions d_t ("absence confirmed," "anomaly detected," or "continue") that rely only on non-sensitive accumulated information $\mathcal{G}_t$. We present Alg. 1 to accomplish this, and characterize both theoretical and empirical properties of its operation, spanning guarantees of minimal information leakage, performance (time to completion), and robustness (high-probability bounds on termination).

IV. METHODOLOGY

The algorithm we propose takes inspiration from randomized, sampling-based motion planners [62], [63] and out-of-distribution detection [64]. For each time step, when a measurement is consistent with source-absence, the robot

moves according to a "reference" random walk (maximum step size c_U) that explores the space; otherwise, if consistent with source-presence, it moves according to an alternative "out-of-distribution" random walk (maximum step size c_L). Detection of a shift in the composite (realized) action distribution is accomplished by Kolmogorov-Smirnov (KS) testing [65]. Since the actions depend only on the detected counts, the resulting distribution over actions (step sizes) for any source-free map is theoretically identical (proven in Sec. V-B); we refer to this source-free action distribution as the reference distribution, V_r.

In practice, we consider a robot that can translate forward and rotate in place (e.g., via encoders on a wheeled system), to detect imminent collisions in a non-destructive fashion (e.g., via very "myopic" distance sensors), and to accurately acquire radiation measurements; such a system can run Alg. 1. Intuitively, the robot "slows down" (takes smaller step sizes) when anomalously high counts (statistically above background) are detected. In this way, legitimate evidence of source-presence is self-reinforcing. We set the reduced step size to $c_L = \frac{c_U}{10}$; for $c_L \lesssim \epsilon_M$, the inspector is likely to stay in the vicinity of an anomalous source. Note that the step size recorded is the randomly-selected distance between measurement points, and *not* the distance between turns; when the robot encounters an obstacle, it randomly redirects and continues to travel the remaining distance.

Algorithm 1 Random walk absence confirmation.

Input: Background count rate B, outer dimensions l_x, l_y, confidence parameter p^*, run time T, test count n, threshold level z, constants $0 \leq c_L < c_U$, reference V_r
Initialize $\underline{p} = 1.0$, $t = 1$, $V_e = \{\emptyset\}$,
$x_0 \sim \mathcal{U}[0, \bar{l}_x]$, $y_0, \sim \mathcal{U}[0, l_y]$, $\theta_0 \sim \mathcal{U}[0, 2\pi]$
while $t \leq T$ **do**
   $N_t \sim h(x_t, y_t; E)$ {Measurement}
   $c \leftarrow c_L + (c_U - c_L)\mathbb{1}[N_t \leq B + z\sqrt{B}]$
   $ds, d\theta \sim \mathcal{U}[0, c], \mathcal{U}[0, 2\pi]$ {Step Length, Rotation}
   Rotate by $d\theta$ rad. and move forward ds distance
   Append ds to memory V_e
   if $t \equiv 0 \pmod{T/n}$ **then**
      $\underline{p} = \min\{\underline{p}, \mathbf{KS}(V_e, V_r)\}$
   end if
   if $\underline{p} \leq p^*/n$ **then**
      return 1   {Anomaly detected}
   end if
end while
return 0   {Absence confirmed}

Note that Alg. 1 requires an estimate of the background radiation. In this work, we assume that the background has been previously characterized (e.g., when the environment was initialized); it could also be learned in a pseudo-online fashion using confidence intervals of the Poisson-distributed counts. We defer this problem to future work.

---

[1]This assumption is not too onerous given that human inspectors also have non-zero extent, and therefore would struggle to explore an overly obstacle-dense map. However, for now, we cannot rival humans in being able to flag certain "adversarial" maps as requiring alternative verification – though they of course would use (sensitive) sensory information to do so.

V. CORRECTNESS AND PRIVACY

Correctness requires guaranteeing a low FNR without compromising the FPR, and vice versa. We begin with an immediate characterization of the false-positive calibration.

Remark 1 (Calibrated False Positive Rate): The FPR of Alg. 1 (i.e., the probability of incorrectly detecting an out-of-distribution anomaly) is less than or equal to p^*. This follows from a union bound applied to the outcomes of n pre-specified KS tests at significance p^*/n.

To address the FNR, full coverage of the environment is necessary to correctly eliminate the possibility of source-presence with high confidence. Unfortunately, standard coverage algorithms typically rely on detailed knowledge of the environment [66]–[68]. Even planners which don't require the environment *a priori* typically maintain a state history, forming a representation of the space (e.g., a rudimentary occupancy map) that is incompatible with the information constraint. Therefore, while less time-efficient, random walk processes are needed to provide necessary exploration while not requiring any environmental information. However, using random walks implies that, to calibrate the FNR, we must be able to validate the walks' coverage time properties.

A. Coverage Properties

In essence, our absence confirmation algorithm is a random walk in continuous space reduced to a discrete graph, as described in Sec. III-B. We require a bound on coverage time (T) that guarantees, with high probability, that the entire accessible environment has been explored. Formally, we desire a function $\mathcal{T}(N) = \max_M T_M \forall M \in \mathbb{M}(l_x, l_y, B, \epsilon_{\underline{M}})$ providing an upper confidence bound on coverage time for a given class of maps. The following lemma characterizes the tail behavior of the distribution governing this quantity.

Lemma 2 (Passage Times in Exponential Family [48]): Consider any compressed map with N nodes (with graph diameter D_G, radius r_G). The distribution of first passage times to a node i from any other node $j \neq i$ is a member of the exponential family (App. VIII-B); namely, the first passage time from node $j^* \neq i$ to node i is distributed geometrically in non-dimensionalized time $\tau = \frac{t}{r_G(i)}$, where $r_G(i) \leq D_G \leq N$. This ensures that relatively tight high-probability bounds on coverage can be obtained (App. VIII-C); it also reflects how the particular structure overcomes several worst-case coverage time results.

To achieve a calibrated FNR, the conditional probability of source detection *given* full graph coverage must also be quantified. This is a multi-faceted (but analytical) problem [69]. In general, utilizing higher efficiency detectors and sampling for longer periods improves the detectable range of source strengths. Henceforth, we assume that sources are sufficiently strong (or, that the detector is sufficiently sensitive within the range r_D) that the conditional probability is essentially equal to one. The results of the hardware experiments in Sec. VI-B are consistent with this assumption.

For now, we assess the coverage time empirically on a diverse set of 10 simulated environments (described further in Sec. VI-A), several of which reflect known worst-case configurations for undirected graphs. We simulate 50 independent trials for each 10×10 m environment and each of 5 different maximum step sizes $c_U = (2, 4, 6, 8, 10$ m$)$. From this, we determine the coverage versus time for a range of discretization sizes (25, 100, or 400 bins of corresponding side length 2, 1, or 0.5 m). We can use these results (summarized in Table I) to approximate $\mathcal{T}(N)$. Figure 2 visualizes the empirical coverage over time for the 5×5 binning; the 25-bin compressed maps are most closely aligned with the hardware experiments of Sec. VI-B.

	2 m	4 m	6 m	8 m	10 m
5×5 bins	810 (3529)	305 (1861)	200 (1721)	159 (818)	145 (699)
10×10 bins	1481 (5285)	741 (2614)	611 (1932)	547 (1444)	547 (1369)
25×25 bins	3422 (12161)	2502 (6710)	2300 (6369)	2256 (6295)	2232 (5022)

TABLE I Empirical coverage time (step number) for varied maximum step size and discretization. The mean number of steps, averaged over all 10 environments and all 50 trials, is reported; the maximum over all rooms and trials is reported in parentheses.
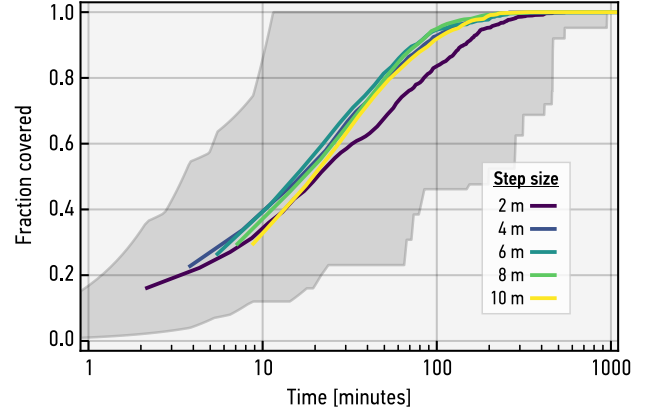
Fig. 2: Empirical coverage versus time for a range of maximum step sizes for the 5×5 binning. For each step size, the average over all 10 environments and all 50 trials is shown; the curves start after 10 initial time steps. The shaded region represents the full range of possible values, evaluated over all step sizes. To convert from step number to real-world time, we assumed 3-second measurements, travel speed of 10 cm/s, and neglect the time spent avoiding obstacles.

B. Information Privacy

In addition to the high-probability coverage and calibrated correctness of our proposed algorithm, a satisfactory verification approach must also be private. Theorem 3 formalizes the privacy of our proposed methodology.

*Theorem 3 (Information Privacy of Compliant Hosts):* Consider the class $\mathbb{M}^-(l_x, l_y, B, \epsilon_{\underline{M}})$ of compliant (source-free) maps. Then Alg. 1 is private, for all time, with respect to any map $M \in \mathbb{M}^-$, in that the mutual information ($\mathcal{MI}$) [70] between any stored data point (namely, the step size between measurements) and the particular compliant (source-free) map is zero (Eq. 2).

$$\mathcal{MI}(\{\mathcal{G}_t \setminus \mathcal{G}_{t-1}\}, \mathbb{M}^-) = \mathcal{MI}(ds_t, \mathbb{M}^-) = 0 \ \forall t \geq 1 \quad (2)$$

In other words, at *no time* in its operation can Alg. 1 distinguish *any pair* of compliant maps (App. VIII-D).

To demonstrate this result, Figure 3 shows (in simulation) that our proposed algorithm, which stores only the step size between measurements, yields an inspection result that depends *only* on the absence or presence of a source, consistent with Theorem 3.[2] Conversely, a seemingly similar information storage scheme which stores the step size between turns (instead of between measurements) "leaks" enough information to differentiate between environments – the stored information is not environment-independent.
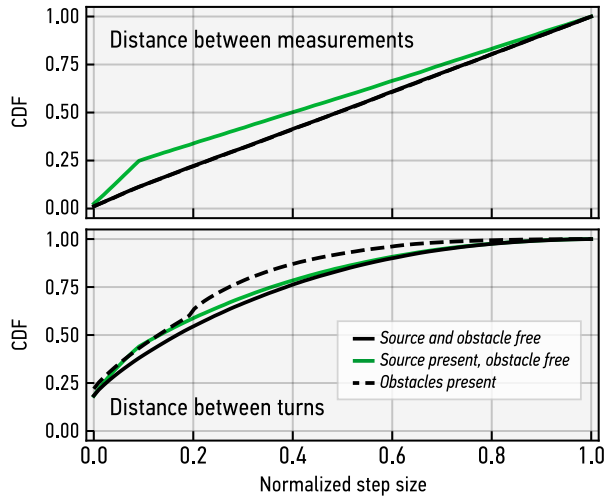
Fig. 3: **Cumulative density functions over step size for our algorithm (distance between measurements) and a "leaky" alternative (distance between turns).** Our algorithm (above) is only dependent on the presence/absence of a source, whereas the seemingly similar information storage scheme (below) leaks information which can differentiate between environments of differing occupancy. Note that the solid and dashed black lines in the upper plot are overlapped; this particular curve is equivalent to the reference distribution, V_r, which is independent of the environment.

VI. EXPERIMENTS

In this section, we demonstrate the correctness of our proposed algorithm, i.e., the ability to correctly identify the absence or presence of a source, both in diverse simulated environments and on hardware in various laboratory settings. Between the simulated and laboratory environments, we test our algorithm on a wide range of scales and configurations.

A. Simulation in PyBullet

Our simulation environment uses PyBullet [71], [72] and is based on the environment setup from [73], which provides an appropriate framework and robot model. A variety of environments were constructed (30 in total, not including the 10 rooms used for empirical results), each with different occupancy functions from several distinct "families." All environments were designed as a 10 m square (outer dimensions), but the open space inside ranges from the full 100 m^2 (empty room) down to 20 m^2; the assortment of environments includes a mix of predominantly open maps and obstacle-dense maps (App. VIII-E).

For each map, 100 independent trials were conducted: 10 with and 10 without a source present, for 5 different maximum step sizes. For each trial, the robot and source (if present) were initialized in random positions within the open space. Ray-tracing provided a realistic, albeit simplified, radiation measurement model, where obstacles are assumed to be fully attenuating and the spatial (distance) dependence for non-attenuated counts was experimentally-based.

The evolution of the KS test significance for Alg. 1, averaged over all similar trials (i.e., 1,500 trials each for source absence and presence) across all environments, is shown in Figure 4. We apply the KS test after every 100 measurements, using $p^* = 0.005$ and $n = 500$, assuming a conservative upper coverage time of 50,000 steps. This yields an overall confidence of 99.5% (0.5% FPR). For omniscient reference, the corresponding average coverage is included; this information is *not* acquired, or even able to be inferred, given the data storage of Alg. 1.
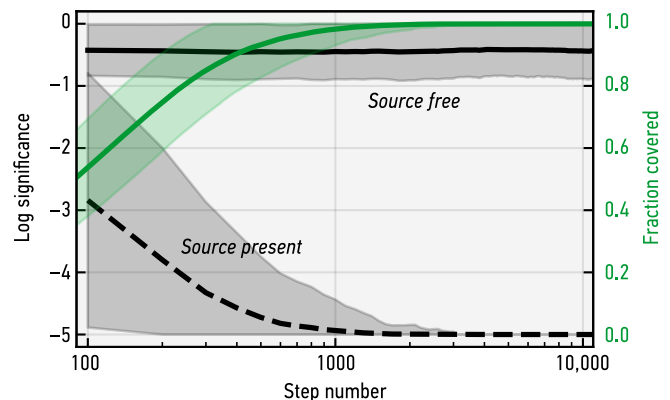
Fig. 4: **Evolution of KS test significance and spatial coverage versus iteration for simulated trials.** The results for source-absence (solid) and source-presence (dashed) are averaged over all trials and simulated rooms. Coverage is shown for the source-absence case; coverage for the source-presence case is omitted since Alg. 1 terminates once a source is confirmed (i.e., coverage is not guaranteed, nor is it necessary, if a source is detected). The log-significance, represented in $\log_{10}$-space, is floored at the KS test trigger threshold, which was -5 for the simulated trials. For each curve, the shaded region represents one standard deviation of the full range of values.

B. Hardware Demonstration

The prototype system developed for this work is built on the iRobot Create 3 platform [74]. Collision avoidance is accomplished using the onboard infrared sensors. The radiation detection unit includes two sensing modalities. For near-range measurements, with the potential for directional sensitivity,[3] three Geiger counters are evenly distributed around the circumference of the robot. We utilize the LND 7314 2in Pancake Geiger detector that is used by the Safecast bGeigie Nano [78]. An Adafruit ESP32 Feather V2 is used to count the pulses from each detector individually, and relay the counts to the controller via Bluetooth. We take the detector range of the Geiger counters to be $r_D = 30\ cm$.

---

[2]Even in the source-presence case, the stored information is secure since the action distribution is essentially a lossy, non-unique convolution of unknown factors (source strength, distance, number of measurements, etc.).

[3]Directional radiation detectors [75], [76] enable a pseudo-random walk policy. In the absence of a prevailing source, the direction is random due to the Poisson counting statistics. If a source is present, the robot more expeditiously switches to the "slowed down" policy, manifesting as noisy gradient ascent, with similar functionality as model-free infotaxis [77].
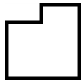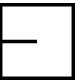
For higher-efficiency, long-range measurements, we use a 2-inch Mirion/Canberra NaI scintillator (Model 802) connected to an Osprey Digital MCA Tube Base [79], [80]. A Raspberry Pi 4 Model B reads the data over Ethernet, and similarly relays the counts to the controller. For rudimentary filtering to improve the signal-to-background ratio by excluding low energy noise, channels ≥ 400 of the 2048-channel spectrum are summed to yield gross counts. The NaI detector has a much larger detector range of conservatively $r_D = 1\ m$. The assembly of the unit (pictured in Figure 1) is designed such that the ring of Geiger counters does not obstruct the solid angle of the NaI crystal.

For source-presence environments, a set of gamma-ray check sources were used (Cs-137, Ba-133, and Co-60, among other isotopes) totaling to around 9 μCi of activity. The experimental analog to Figure 4 is shown in Figure 5 for two full-scale environments (20 m^2 rectangle and 22 m^2 L-shape) using the NaI detector and 1 m^2 bins. We apply the KS test after every 20 measurements, using $p^* = 0.005$ and $n = 50$, assuming an upper coverage time of 1000 steps. As before, this yields an overall confidence of 99.5%.
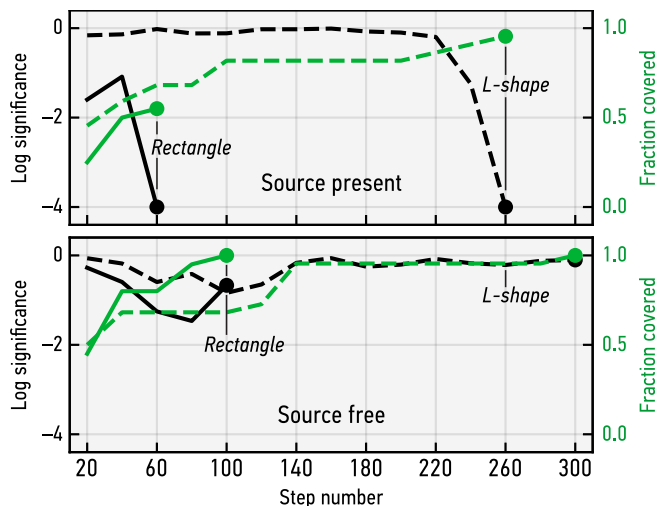
Fig. 5: Evolution of KS test significance and spatial coverage for two representative full-scale experimental environments. For the source-presence cases (above), the time step when Alg. 1 terminates is indicated (i.e., once the KS test log-significance, represented in $\log_{10}$-space, reaches -4). For the source-absence cases (below), the time step when coverage is first reached is indicated; note that the algorithm would *not* terminate in this case, since coverage is not known to the inspector.

In addition to the large-scale environments, we conducted a series of experiments in rooms of varying complexity and connectivity. Four laboratory environments are summarized in Table II, all using the NaI detector and 1 m^2 bins, each with a different open area and structure. For all trials in all environments, Alg. 1 yields the correct result: when no source was present, the robot covered the environment without returning a significant KS test; when a source was present, the robot more expeditiously returned a significant KS test result, indicative of an anomalous source. As seen in Figure 5 and Table II, if a source was present, the KS test causes Alg. 1 to terminate in fewer steps than necessary to achieve full coverage of the search environment.

	14 m^2	12 m^2	16 m^2	13 m^2
Simulated cover time	166 ± 47	125 ± 59	265 ± 131	171 ± 63
Hardware cover time	76 ± 22	82 ± 36	94 ± 22	128 ± 42
KS time for source	39 ± 15 (52 ± 16)	50 ± 17 (56 ± 20)	60 ± 37 (72 ± 35)	34 ± 6 $(40 \pm 0)^\dagger$

TABLE II Key metrics for laboratory trials. For the four environments, the number of steps to reach full coverage for the no-source case and the steps to the first instance of $\log_{10}(P) = -4$ for the source case is reported; each table entry includes the average and standard deviation over 5 trials. Note that for our chosen test parameters (1000 maximum steps, 50 KS tests), Alg. 1 can only return a significant KS test result after every 20 steps; the corresponding time to the algorithm terminating is in parentheses. For reference, the experimental configurations were reproduced in PyBullet; the corresponding coverage time for 10 trials is reported. †For all 5 source trials in the 13 m^2 environment, the KS test triggered after 40 measurements.

To briefly demonstrate the utility of a detector with larger range r_D, we compare the performance of the two sensing modalities. We caution that the conservative obstacle avoidance of the Create 3 compounds with the limited range of the Geiger counters, thereby making it very difficult (and unlikely) that the robot remains in the vicinity of the source for long enough to trigger the KS test. Nonetheless, in a relatively small space measuring 2×4 m, the Geiger counters required 3.33-times more steps than the NaI-equipped robotic inspector for Alg. 1 to correctly terminate with $d = 1$ (anomaly detected). Similarly, coverage with the NaI detector was achieved 2.54-times faster than with the Geiger counters.

VII. DISCUSSION

This work underscores the prospect and fundamental challenge of deploying robotic radiation detectors for nuclear verification, where security is imperative and information leakage must be minimized. We established a privacy-preserving approach which demonstrates the ability to perform high-confidence source verification tasks without requiring nor providing any information about the search environment.

The constraints of finite time, complex or large environments, and detector efficiency may be addressed by limited, rather than minimal, information approaches. Quantifying this trade-off between permissible information and inspection efficiency remains an interesting research topic. As a future extension, the KS testing may also be used to confirm that an environment is unchanged by redefining the reference distribution (i.e., template matching). Alternatively, by increasing the situational awareness of the robot, limited contextual knowledge can afford the intuition that a radioactive source must be bound to a sufficiently substantial physical feature.

ACKNOWLEDGMENTS

VIII. APPENDIX

A. Discretization Procedure

Consider map M with occupancy function $f'(x,y)$: $[0,l_x] \times [0,l_y] \mapsto \{0,1\}$ associating all points within the outer bounds to "free space" (0) or "not free space" (1). Let $\epsilon_M \geq 0$ be the "fundamental discretization length" of map M, defined to be the largest $\epsilon \in \mathbb{R}^{\geq 0}$ such that there is a discretization of the occupancy function into bins $\{b_i\}_{i=1}^{N(\epsilon)}$ of side length at least ϵ with the following properties: (1) the modified, *conservative* occupancy function is $f(i) = \max_{x,y \in b_i}\{f'(x,y)\}$, and (2) the resulting discretized map is traversable by inspector $\mathcal{I}$. Implicitly, this restricts us to maps with $\epsilon_M = \Omega(r_I)$ and a maximum number of bins $N(\epsilon_M) = \mathcal{O}\left(\frac{l_x l_y}{r_I^2}\right)$. The discretization length is also limited by the detector range: $\epsilon_M \lesssim \frac{r_D}{\sqrt{2}}$, where r_D is the distance from which a source is readily detectable, with the corresponding minimum number of bins $N(\epsilon_M) = \Omega\left(\frac{l_x l_y}{r_D^2}\right)$.

B. Exponential Family

To the best of our knowledge, this result is not a trivial application of eigenvalue theory for directed graphs, nor of Perron-Frobenius theory on graph transition matrices. We believe that the conductance arguments of [48] apply here to give tighter bounds (using the local structure of the physically grounded random walk). For completeness, in case the above results do not apply in an edge case, we give a looser lower bound below.

Proof: By assumption, we are tasked with exploring a contiguous (traversable) space; this translates to the resulting graph representation being strongly connected. Furthermore, because our algorithm allows for small step sizes (down to zero), the probability of self-loops is positive for every node. As such, the graph representation is necessarily aperiodic. From this, first, Perron-Frobenius theory gives that for a strongly connected, aperiodic graph, the associated transition matrix has a unique, positive stationary distribution. Denote this as $\pi_G > 0$. Second, from strong connectivity, the graph diameter (D_G) is less than or equal to N. It follows that, for any node i, the radius of the graph $r_G(i)$ (the maximal distance of any node $j \neq i$ to node i) is necessarily greater than zero and less than or equal to D_G.

The rest is relatively straightforward. Set the output of a state i (the ith column of $\mathbb{P}$, using the convention $\pi_G = \mathbb{P}\pi_G$) to be uniformly zero (such that i is, essentially, an absorbing node). Let the path from the node farthest from i (denote this as $j^*(i)$) to i be defined as $\{j_k\}_{k=0}^{r_G(i)}$, where $j_0 = j^*(i)$ and $j_{r_G(i)} = i$. Then after $r_G(i)+1$ steps, for any $v_0 \in \Delta_N$, $\|\mathbb{P}^{r_G(i)+1}v\|_1 \leq 1 - c(i)$, where $c(i) = \Pi_{k=1}^{r_G(i)}\mathbb{P}_{j_k \leftarrow j_{k-1}}$. Let $\lambda(i) = 1 - c(i) < 1$, and denote a non-dimensionalized time $\tau = t/r_G(i)$. We can interpret the one-norm of the vector $v_\tau(v_0)$ as follows: the upper bound of the probability of not having reached state i in time τ, given that we have started in (proper, normalized) state distribution v_0. This function has the form $F_0(\tau) = \lambda^\tau$. It is, therefore, clear that the (lower bound) cumulative distribution function of the first passage time is $F(t) = 1 - F_0(\tau) = 1 - \lambda(i)^\tau = 1 - \lambda(i)^{t/r}$. Because t is discrete, this can be modeled as a geometric distribution in non-dimensionalized time τ, or in $\lfloor \frac{t}{r_G(i)} \rfloor$. ∎

C. Efficient High-Probability Bounds on Coverage Time

Below, we provide a means of generating high-probability bounds on coverage time demonstrating that coverage is dominated by worst-case cover time of a particular node, consistent with other work in the literature. Furthermore, significantly better bounds (empirically) can be obtained by leveraging the exponential family properties of the cover time distribution as compared to less restrictive bounds (e.g., Markov's Inequality, which only requires a bound on the first moment of the distribution).

In essence, the method utilizes an informative prior: reaching adjacent nodes should have relatively strong correlation. Consider a physical, discretized map with N nodes v_n. Partition the nodes into $N/2$ disjoint subsets $b_i = \{v_{n_i,1}, v_{n_i,2}\}$ of two nodes each (in this and all ensuing steps, if the number of input nodes is odd, there will be $(N+1)/2$ output subsets, where the last subset is singleton and will be incorporated in a subsequent step). Define for each output subset b_i the following conditional event: the output subset b_i is fully explored at or before time $t_0 + \tau$ with probability greater than $1 - \delta/(N)$, given that at least one node within b_i has been reached at time t_0. This is equivalent, for each subset, to $\max\{\bar{t}_{1\rightarrow 2}, \bar{t}_{2\rightarrow 1}\}$, the respective times to traverse from the first node in b_i to the second, and from the second to the first, each with probability $1 - \delta/(2N)$. Associate the above maximum time with bin b_i; by a union bound over the two possibilities, the maximum time holds with probability $1 - \delta/N$. Note that there are $N/2$ such bins.

Now, we simply repeat the process, using the previous output subset as the input nodes. That is, bins b_i are the $N/2$ input "nodes," and we can let b_j be the $N/4$ output subsets. Let $b_j = \{b_1^{[j]}, b_2^{[j]}\}$; now, the integration requires us to consider the maximum over four possibilities: (1) exploring $b_1^{[j]}$, (2) exploring $b_2^{[j]}$, (3) going from $b_1^{[j]}$ to $b_2^{[j]}$ and then exploring $b_2^{[j]}$, and (4) going from $b_2^{[j]}$ to $b_1^{[j]}$ and then exploring $b_1^{[j]}$. The first two exploration possibilities are strictly dominated by the last two, so with each b_j we associate the value $\max\{\bar{t}_{1\rightarrow 2}+\bar{t}_2, \bar{t}_{2\rightarrow 1}+\bar{t}_1\}$. This is the same as the first step, except that in the first step the associated "accumulated times" (i.e., the time traveling from one node to the next) were zero, and left implicit. Assuming that the traversals are bounded again by probability $1 - \delta/(2N)$, the union bound (combined with the existing ones from preceding steps) bounds the outcomes for the further-reduced b_j.

Zooming out, we can imagine that repeating this process for $\lceil \log_2(N) \rceil$ steps is guaranteed to result in a single remaining bin. Summing over combinations, we have that there are N combinations made $(N/2 + N/4 + ...)$ and that each combination adds two union bounds. Therefore, there are $2N$ union bounds, and the resulting, consolidated "maximum of maximums" is an upper bound with probability greater than $1 - \delta$. As such, the resulting high-confidence upper bound is

$\mathcal{O}(\bar{T} \log N)$, where $\bar{T}$ is the worst case (over the N "real" nodes) upper bounded cover time for a single node.

A key intuition that we rely upon here is the actual realization of the bin partition; physical proximity is a strong prior for the mixing of physical random walks, which allows for useful speed-up. Concretely, we can construct a partition of pairs of physically adjacent bins which mixes faster than a partition of randomly selected pairs of bins. Second, this intuition also suggests that an optimal step size (from the perspective of obtaining upper bounds) should exist and that it should not be too large, as a large step size – beyond taking more time to execute – weakens the prior over good partition pairs. Therefore, this reflects the implicit trade-off between quick exploration at large scales (which benefits from larger step sizes) and thorough exploration at smaller scales (which benefits from smaller step sizes).

D. Mutual Information

Proof: Consider normalized step constants $c'_U = 1$, $c'_L = c_L/c_U$, and similarly normalized step sizes $V'_e = V_e/c_U$. Let $\delta(z) \in (0, 1]$ denote the one-sided significance of the quantile $c(z) = B + z\sqrt{B}$ for a Poisson distribution with mean and variance B. That is, for random variables $X_i \overset{\text{iid}}{\sim}$ Poisson(B), $\delta(z) := \mathcal{P}(X >= c(z))$.

It can be shown that in source-free environments, the step-size density function $q_{\delta(z)}(s|m^-, b)$ is equal to $(c'_L + \delta(z) - c'_L \delta(z))/c'_L$ for $s \in [0, c'_L]$ and $(1 - \delta(z))$ for $s \in [c'_L, 1]$, equal to the marginal no-source density $p_{\delta(z)}(s)$. This is due to the uniformity across bins of the count rate distribution. From this, the proof follows by direct decomposition of the mutual information and reduction of the joint probability distribution. By definition,

$$\mathcal{MI}(dx_t, M^-) := KL(q_{\delta(z)}(s, M^-)\|p_{\delta(z)}(s)p(M^-)).$$

For any $\{s, M^-\}$, $q_{\delta(z)}(s, M^-) = q_{\delta(z)}(s|M^-)p(M^-)$. By the law of iterated expectation, this can be expanded to individual bins in the map as follows:

$$q_{\delta(z)}(s|M^-)p(M^-) = \mathbb{E}_{b \sim \mu_{(M^-)}}\left[q_{\delta(z)}(s|M^-, b)\right]$$

But this latter term is precisely the density function described above, which is independent of $\{M^-, b\}$ and depends solely on $\delta(z)$ (when there is no source). Therefore:

$$\begin{aligned} q_{\delta(z)}(s|M^-) &= \mathbb{E}_{b \sim \mu_{(M^-)}}\left[q_{\delta(z)}(s|M^-, b)\right] \\ &= q_{\delta(z)}(s|M^-, b) \\ &= p_{\delta(z)}(s) \end{aligned}$$

Therefore, $q_{\delta(z)}(s|M^-) = p_{\delta(z)}(s)$, and we recover the expression for the mutual information:

$$\begin{aligned} \mathcal{MI}(dx_t, M^-) &:= KL(q_{\delta(z)}(s, M^-)\|p_{\delta(z)}(s)p(M^-)) \\ &= KL(q_{\delta(z)}(s|M^-)p(M^-)\|p_{\delta(z)}(s)p(M^-)) \\ &= KL(p_{\delta(z)}(s)p(M^-)\|p_{\delta(z)}(s)p(M^-)) \\ &= 0. \end{aligned}$$

Importantly, we note that this result is true for *any* probability law over the set of source-free maps; in particular, this holds uniformly across all maps (which can be seen by taking the set of probability laws that place all of their mass on a particular map). ∎

E. Simulation Environments
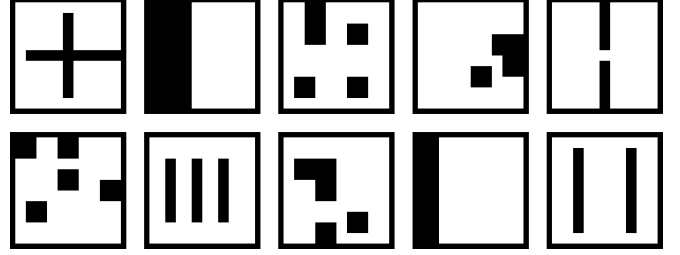
Fig. 6: Selection of a simulated environments with varying complexity. All rooms are designed with the same 10×10 m outer dimensions with different occupancy fractions and obstacle shapes.

REFERENCES

[1] *IAEA Safeguards: Serving Non-Proliferation*, International Atomic Energy Agency, 2018.

[2] J. Carlson, V. Kuchinov, and T. Shea, *The IAEA's Safeguards System as the Non-Proliferation Treaty's Verification Mechanism*, May 2020.

[3] J. Fuller, "Verification on the Road to Zero: Issues for Nuclear Warhead Dismantlement," Arms Control Today, December 2010.

[4] C. Comley, M. Comley, P. Eggins, G. George, S. Holloway, M. Ley, P. Thompson, and K. Warburton, *Confidence, Security & Verification, The Challenge of Global Nuclear Weapons Arms Control*, AWE/TR/2000/001, Atomic Weapons Establishment, Aldermaston, United Kingdom, 2000.

[5] *Radiation Detection Equipment: An Arms Control Verification Tool*, Product No. 211P, Defense Threat Reduction Agency, Fort Belvoir, VA, October 2011.

[6] National Academies of Sciences, Engineering, and Medicine, *Nuclear Proliferation and Arms Control Monitoring, Detection, and Verification: A National Security Priority: Interim Report*, The National Academies Press, 2021.

[7] F. F. Dean, *ROBIN: A Way to Collect In-Plant Safeguards Data with Minimal Inspector Access*, SAND82-1588C, Sandia National Laboratories, 1982.

[8] K. Robertson, R. Stohr, A. Elfes, P. Flick, A. Sokolov, D. Finker, and C. Everton, "The IAEA Robotics Challenge – Demonstrating Robots for Safeguards Inspections," IAEA Symposium on International Safeguards: Building Future Safeguards Capabilities, IAEA-CN-267/215, 2018.

[9] F. E. Schneider and D. Wildermuth, "Real-World Robotic Competitions for Radiological and Nuclear Inspection Tasks," *20th International Carpathian Control Conference (ICCC)*, pp. 1-6, 2019.

[10] B. Bird, A. Griffiths, H. Martin, E. Codres, J. Jones, A. Stancu, B. Lennox, S. Watson, and X. Poteau, "A Robot to Monitor Nuclear Facilities: Using Autonomous Radiation-Monitoring Assistance to Reduce Risk and Cost," *IEEE Robotics & Automation Magazine*, vol. 26, no. 1, pp. 35-43, 2019.

[11] R. Smith, E. Cucco, and C. Fairbairn, "Robotic Development for the Nuclear Environment: Challenges and Strategy," *Robotics*, vol. 9 no. 4, 94, 2020.

[12] M. Chiou, G. T. Epsimos, G. Nikolaou, P. Pappas, G. Petousakis, S. Mühl, and R. Stolkin, "Robot-Assisted Nuclear Disaster Response: Report and Insights from a Field Exercise," *IEEE/RSJ International Conference on Intelligent Robots and Systems (IROS)*, 2022.

[13] I. Tsitsimpelis, C. J. Taylor, B. Lennox, and M. J. Joyce, "A Review of Ground-Based Robotic Systems for the Characterization of Nuclear Environments," *Progress in Nuclear Energy*, vol. 111, pp. 109-124, 2019.

[14] F. Gagliardi, "Integration of Independent NDA Techniques within a SLAM-based Robotic System for Improving Safeguards Standard Routines: A Review of the Current Status and Possible Future Developments," *ESARDA Bulletin*, vol. 64, no. 2, pp. 10-21, 2022.

[15] D. Hellfeld, T. H. Y. Joshi, M. S. Bandstra, R. J. Cooper, B. J. Quiterm, and K. Vetter, "Gamma-Ray Point-Source Localization and Sparse Image Reconstruction Using Poisson Likelihood," *IEEE Transactions on Nuclear Science*, vol. 66, no. 9, pp. 2088-2099, 2019.

[16] J. R. Vavrek, D. Hellfeld, M. S. Bandstra, V. Negut, K. Meehan, W. J. Vanderlip, J. W. Cates, R. Pavlovsky, B. J. Quiter, R. J. Cooper, and T. H. Y. Joshi, "Reconstructing the Position and Intensity of Multiple Gamma-Ray Point Sources with a Sparse Parametric Algorithm," *IEEE Transactions on Nuclear Science*, vol. 67, no. 11, pp. 2421-2430, 2020.

[17] F. Mascarich, P. D. Petris, H. Nguyen, N. Khedekar, and K. Alexis, "Autonomous Distributed 3D Radiation Field Estimation for Nuclear Environment Characterization," *IEEE International Conference on Robotics and Automation (ICRA)*, pp. 2163-2169, 2021.

[18] F. Mascarich, M. Kulkarni, P. De Petris, T. Wilson, and K. Alexis, "Autonomous mapping and spectroscopic analysis of distributed radiation fields using aerial robots," *Autonomous Robots*, vol. 47, pp. 139-160, 2023.

[19] A. West, I. Tsitsimpelis, M. Licata, A. Jazbec, L. Snoj, M. J. Joyce, and B. Lennox, "Use of Gaussian process regression for radiation mapping of a nuclear reactor with a mobile robot," *Scientific Reports*, vol. 11, 13975, 2021.

[20] N. A. Abd Rahman, K. S. M. Sahari, N. A. Hamid, and Y. C. Hou, "A coverage path planning approach for autonomous radiation mapping with a mobile robot," *International Journal of Advanced Robotic Systems*, vol. 19, no. 4, 2022.

[21] K. Groves, E. Hernandez, A. West, T. Wright, and B. Lennox, "Robotic Exploration of an Unknown Nuclear Environment Using Radiation Informed Autonomous Navigation," *Robotics*, vol. 10, no. 2, 78, 2021.

[22] E. Lepowsky, J. Jeon, and A. Glaser, "Confirming the Absence of Nuclear Warheads via Passive Gamma-Ray Measurements," *Nuclear Instruments and Methods in Physics Research Section A: Accelerators, Spectrometers, Detectors and Associated Equipment*, vol. 990, 164983, 2021.

[23] R. Aylett and P. A. Vargas, "11. Social Interaction: Pets, Butlers, or Companions?" In *Living with robots: What every anxious human needs to know*, MIT Press, 2023.

[24] B. Ristic, M. Morelande, and A. Gunatilaka, "Information driven search for point sources of gamma radiation," *Signal Processing*, vol. 90, no. 4, pp. 1225-1239, 2010.

[25] E. A. Miller, S. M. Robinson, K. K. Anderson, J. D. McCall, A. M. Prinke, J. B. Webster, and C. E. Seifert, "Adaptively Reevaluated Bayesian Localization (ARBL): A novel technique for radiological source localization," *Nuclear Instruments and Methods in Physics Research Section A: Accelerators, Spectrometers, Detectors and Associated Equipment*, vol. 784, pp. 332-338, 2015.

[26] R. B. Anderson and M. Pryor, "Mobile Robotic Radiation Surveying with Recursive Bayesian Estimation and Attenuation Modeling," *IEEE Transactions on Automation Science and Engineering*, vol. 19, no. 1, 410-424, 2022.

[27] R. B. Anderson, C. Pehlivantürk, and M. Pryor, "Optimization Strategies for Bayesian Source Localization Algorithms," *IEEE Transactions on Automation Science and Engineering*, vol. 20, no. 1, pp. 394-403, 2023.

[28] G. Cordone, R. R. Brooks, S. Sen, N. S.V. Rao, C. Q. Wu, M. K. Berry, and K. M. Grieme, "Improved multi-resolution method for MLE-based localization of radiation sources," *20th International Conference on Information Fusion*, 2017.

[29] E.W. Bai, K. Yosief, S. Dasgupta, and R. Madumbai, "The maximum likelihood estimate for radiation source localization: Initializing an iterative search," *53rd IEEE Conference on Decision and Control*, pp. 277-282, 2014.

[30] P. Proctor, C. Teuscher, A. Hecht, and M. Osiński, "Proximal Policy Optimization for Radiation Source Search," *Journal of Nuclear Engineering*, vol. 2, no. 4, pp. 368-397, 2021.

[31] Z. Liu and S. Abbaszadeh, "Double Q-Learning for Radiation Source Detection," *Sensors*, vol. 19, no. 4, 960, 2019.

[32] M. S. Bandstra, D. Hellfeld, J. R. Vavrek, B. J. Quiter, K. Meehan, P. J. Barton, J. W. Cates, A. Moran, V. Negut, R. Pavlovsky, and T. H. Y. Joshi, "Improved Gamma-Ray Point Source Quantification in Three Dimensions by Modeling Attenuation in the Scene," *IEEE Transactions on Nuclear Science*, vol. 68, no. 11, pp. 2637-2646, 2021.

[33] G. Christie, A. Shoemaker, K. Kochersberger, P. Tokekar, L. McLean, and A. Leonessa, "Radiation search operations using scene understanding with autonomous UAV and UGV," *Journal of Field Robotics*, vol. 34, pp. 1450–1468, 2017.

[34] D. P. Kingma and M. Welling, "An Introduction to Variational Autoencoders," *Foundations and Trends in Machine Learning*, vol. 12, no. 4, pp. 307-392, 2019.

[35] P. Vincent, H. Larochelle, I. Lajoie, Y. Bengio, and P.A. Manzagol, "Stacked Denoising Autoencoders: Learning Useful Representations in a Deep Network with a Local Denoising Criterion," *Journal of Machine Learning Research*, vol. 11, no. 110, pp. 3371-3408, 2010.

[36] D. P. Kingma and M. Welling, "Auto-Encoding Variational Bayes," arXiv:1312.6114, 2022.

[37] M. Booker and A. Majumdar, "Switching Attention in Time-Varying Environments via Bayesian Inference of Abstractions," *IEEE International Conference on Robotics and Automation (ICRA)*, pp. 10174-10180, 2023.

[38] V. Pacelli and A. Majumdar, "Robust Control Under Uncertainty via Bounded Rationality and Differential Privacy," *IEEE International Conference on Robotics and Automation (ICRA)*, pp. 3467-3474, 2022.

[39] M. Booker and A. Majumdar, "Learning to Actively Reduce Memory Requirements for Robot Control Tasks," *Proceedings of the 3rd Conference on Learning for Dynamics and Control*, PMLR, vol. 144, 2021.

[40] Y. Xu, S. Zhao, J. Song, R. Stewart, and S. Ermon, "A Theory of Usable Information under Computational Constraints," *International Conference on Learning Representations*, 2020.

[41] A. Majumdar, Z. Mei , and V. Pacelli, "Fundamental limits for sensor-

based robot control," *The International Journal of Robotics Research*, 2023.

[42] C. Dwork and A. Roth, "The Algorithmic Foundations of Differential Privacy," *Foundations and Trends in Theoretical Computer Science*, vol. 9, no. 3-4, pp. 211-407, 2013.

[43] C. Dwork, F. McSherry, K. Nissim, and A. Smith, "Calibrating Noise to Sensitivity in Private Data Analysis," S. Halevi and T. Rabin (Eds.), *Theory of Cryptography*, TCC 2006, pp. 265-284, "Lecture Notes in Computer Science," vol. 3876, Springer, Berlin, Heidelberg, 2006.

[44] F. McSherry and K. Talwar, "Mechanism Design via Differential Privacy," *Proceedings of the 48th Annual IEEE Symposium on Foundations of Computer Science (FOCS'07)*, pp. 94-103, 2007.

[45] D. Aldous, "An Introduction to Covering Problems for Random Walks on Graphs," *Journal of Theoretical Probability*, vol. 2, pp. 87-99, 1989.

[46] R. Aleliunas, R. M. Karp, R. J. Lipton, L. Lovasz, and C. Rackoff, "Random Walks, Universal Traversal Sequences, and the Complexity of Maze Problems," *20th Annual Symposium on Foundations of Computer Science (SFCS)*, pp. 218-223, 1979.

[47] D. Aldous and P. Diaconis, "Strong uniform times and finite random walks," *Advances in Applied Mathematics*, vol. 8, no. 1, pp. 69-97, 1987.

[48] M. Mihail, "Conductance and convergence of Markov chains-a combinatorial treatment of expanders," *30th Annual Symposium on Foundations of Computer Science*, pp. 526-531, 1989.

[49] A. Sinclair and M. Jerrum, "Approximate counting, uniform generation and rapidly mixing markov chains extended abstract," H. Göttler and H.J. Schneider (Eds.), *Graph-Theoretic Concepts in Computer Science*, WG 1987, pp. 134-148, "Lecture Notes in Computer Science," vol. 314, Springer, Berlin, Heidelberg, 1988.

[50] F. Ball, B. Dunham, and A. Hirschowitz, "On the Mean and Variance of Cover Times for Random Walks on Graphs," *Journal of Mathematical Analysis and Applications*, vol. 207, no. 2, pp. 506-514, 1997.

[51] S. M. Ross, *Introduction to Probability Models*, 10th ed., Elsevier, Amsterdam, 2010.

[52] E. Seneta, *Non-negative Matrices and Markov Chains*, "Springer Series in Statistics," Springer, New York, 1981.

[53] D. Serre, *Matrices: Theory and Applications*, "Graduate Texts in Mathematics," vol. 216, Springer, New York, 2010.

[54] J.-Q. Dong, W.-H. Han, Y. Wang, X.-S. Chen, and L. Huang, "Universal cover-time distribution of heterogeneous random walks," *Physical Review E.*, vol. 107, no. 2, 024128, 2023.

[55] M. Chupeau, O. Bénichou, and R. Voituriez, "Cover times of random searches," *Nature Physics*, vol. 11, no. 10, pp. 844-847, 2015.

[56] L. Régnier, M. Dolgushev, S. Redner, and O. Bénichou, "Universal exploration dynamics of random walks," *Nature Communications*, vol. 14, no. 1, 618, 2023.

[57] A. Sharma, N. Azizan, and M. Pavone, "Sketching curvature for efficient out-of-distribution detection for deep neural networks," *Proceedings of the Thirty-Seventh Conference on Uncertainty in Artificial Intelligence*, PMLR, pp. 1958–1967, 2021.

[58] R. Sinha, A. Sharma, S. Banerjee, T. Lew, R. Luo, S. M. Richards, Y. Sun, E. Schmerling, and M. Pavone, "A System-Level View on Out-of-Distribution Data in Robotics," arXiv:2212.14020, 2022.

[59] A. Farid, D. Snyder, A. Z. Ren, and A. Majumdar, "Failure Prediction with Statistical Guarantees for Vision-Based Robot Control," arXiv:2202.05894, 2022.

[60] A. Farid, S. Veer, B. Ivanovic, K. Leung, and M. Pavone, "Task-Relevant Failure Detection for Trajectory Predictors in Autonomous Vehicles," *Proceedings of the 6th Conference on Robot Learning (PMLR)*, vol. 205, pp. 1959-1969, 2023.

[61] R. Luo, S. Zhao, J. Kuck, B. Ivanovic, S. Savarese, E. Schmerling, and M. Pavone, "Sample-Efficient Safety Assurances Using Conformal Prediction," S. M. LaValle, J. M. O'Kane, M. Otte, D. Sadigh, and P. Tokekar (Eds.), *Algorithmic Foundations of Robotics XV*, WAFR 2022, pp. 149-169, "Springer Proceedings in Advanced Robotics," vol. 25, Springer, Cham, 2022.

[62] S. M. LaValle and J. J. Kuffner, "Randomized Kinodynamic Planning," *International Journal of Robotics Research*, vol. 20, no. 5, pp. 378-400, 2001.

[63] J. J. Kuffner and S. M. LaValle, "RRT-Connect: An Efficient Approach to Single-Query Path Planning," *IEEE International Conference on Robotics and Automation (ICRA)*, vol. 2, pp. 995-1001, 2000.

[64] M. Basseville, "Detecting Changes in Signals and Systems – A Survey," *Automatica*, vol. 24, no. 3, pp. 309-326, 1988.

[65] A. N. Kolmogorov, "Sulla Determinazione Empirica di Una Legge di Distribuzione," *Giornale dell'Istituto Italiano degli Attuari*, vol. 4, pp. 83-91. 1933

[66] Y. Cao, Y. Han, J. Chen, X. Liu, Z. Zhang, and K. Zhang, "Optimal Coverage Path Planning Algorithm of the Tractor-formation Based on Probabilistic Roadmaps," *IEEE International Conference on Unmanned Systems and Artificial Intelligence (ICUSAI)*, pp. 27-32, 2019.

[67] Z. Khanam, S. Saha, D. Ognibene, K. McDonald-Maier, and S. Ehsan, "An Offline-Online Strategy for Goal-Oriented Coverage Path Planning using A Priori Information," *14th IEEE International Conference on Industry Applications (INDUSCON)*, pp. 874-881, 2021.

[68] S. A. Sadat, J. Wawerla, and R. Vaughan, "Fractal trajectories for online non-uniform aerial coverage," *IEEE International Conference on Robotics and Automation (ICRA)*, pp. 2971-2976, 2015.

[69] G. F. Knoll, *Radiation Detection and Measurement*, 4th ed., Wiley, New York, 2010.

[70] T. M. Cover and J. A. Thomas, *Elements of Information Theory*, John Wiley & Sons, New York, 1991.

[71] E. Coumans and Y. Bai, "PyBullet, a Python module for physics simulation for games, robotics and machine learning," `http://pybullet.org`, 2016–2021.

[72] B. Ellenberger, "PyBullet Gymperium," `https://github.com/benelot/pybullet-gym`, 2018–2019.

[73] Y. Kadhi, V. Lim, D. Zheng, and S. Doncieux, "Learning and generalization on a navigation task of a wheeled robot", `https://github.com/Yurof/WheeledRobotSimulations/`, 2021.

[74] iRobot, "Create 3 Docs," `https://iroboteducation.github.io/create3_docs/`, 2021–2023.

[75] F. Mascarich, C. Papachristos, T. Wilsonm, and K. Alexis, "Distributed Radiation Field Estimation and Informative Path Planning for Nuclear Environment Characterization," *IEEE International Conference on Robotics and Automation (ICRA)*, pp. 2318-2324, 2019.

[76] E. Lepowsky, M. Kütt, S. Aslam, H. Fetsch, S. Snell, A. Glaser, and R. J. Goldston, "Experimental Demonstration and Modeling of a Robotic Neutron Detector with Spectral and Directional Sensitivity for Treaty Verification," *Nuclear Instruments and Methods in Physics Research Section A: Accelerators, Spectrometers, Detectors and Associated Equipment*, vol. 1041, 167362, 2022.

[77] M. Vergassola, E. Villermaux, and B. Shraiman, "'Infotaxis' as a strategy for searching without gradients," *Nature*, vol. 445, pp. 406-409, 2007.

[78] A. Brown, P. Franken, S. Bonner, N. Dolezal, and J. Moross. "Safecast: successful citizen-science for radiation measurement and communication after Fukushima," *Journal of Radiological Protection*, vol. 36, no. 2, pp. S82-S101, 2016.

[79] Mirion Technologies, "802 Scintillation Detectors Data Sheet," 2017.

[80] Mirion Technologies, "Osprey: Universal Digital MCA Tube Base for Scintillation Spectrometry Data Sheet," 2017.